J. Nano.- Electron. Phys.
1 (2009) No1, P. 71-91

PACS numbers: 41.75.Ak; 07.75. + h; 68.55.Ln

MASS-SPECTROMETRIC RESEARCH OF ION SPUTTERING PROCESSES AT HIGH PRIMARY ION ENERGIES

V.A. Baturin, S.A. Yeryomin

Institute of Applied Physics, National Academy of Sciences of Ukraine,
58, Petropavlivs'ka Str., 40030, Sumy, Ukraine

The article is devoted to mass-spectrometric investigation of ion sputtering processes in a wide range of primary ion energies. For this purpose a design of the secondary neutral mass-spectrometer is developed, which unlike the traditional devices of the given type is produced on the base of ion implanter that generates ion beams with energies up to 170 keV and current density on the target up to 1 mA/cm². Computer simulation of the electron and positively charged ion trajectories in sputtered particle detection system is performed and the optimal parameters of a system for three modes of operation are determined. The emission of sputtered neutral copper clusters and the preferential sputtering processes of molybdenum isotopes at different parameters of the primary ion beam are studied.

Keywords: *ION BEAM, SPUTTERING, SECONDARY NEUTRALS, CLUSTER, ISOTOPE, MASS-SPECTROMETER.*

(Received 27 April 2009, in final form 26 June 2009)

1. INTRODUCTION

The problems of atom and molecule emission from target under the action of ion bombardment attract attention of a large number of researchers. This is conditioned both by the physical interest to the process itself and the lots of known applied problems [1-7]. Some of the problems on the ion sputtering physics require the mass separation of ion sputtering products. These problems include, for example, the study of cluster and molecular compound emission, the preferential sputtering of elements of a multielement sample or isotopes of an element.

Thus, in cluster ion sources of sputtering type, it is preferably to use such parameters of primary ion beam for which the cluster fraction in sputtered particle flow is maximal. According to theoretical concept of neutral cluster emission during the sputtering the cluster emission intensity is higher, the higher the ion sputtering coefficient of material, which, in turn, depends on energy of primary ion beam. For example, for widely used for bombardment the ions of inert gases (Ar^+, Kr^+, Xe^+) the maximum of sputtering coefficient is in the range from some tens to some hundreds keV depending on target material [1, 4, 6].

In connection with intensive development of ion lithography technique in microelectronics, which uses beams of light ions with energy of the order of 200 keV, there is a need of detailed study of ion sputtering products of technological and construction materials under given energies of primary ion beam. In modern investigations of controlled thermonuclear synthesis the investigation objectives of erosion products of structural materials by high-intensity flows of charged particles appear as well. Thus, in international work-in-progress ITER the energy of ions, interacting with construction materials, can lead hundreds of keV.

Another important research area in the ion sputtering physics, which requires a mass analysis of particles, is preferential sputtering of the test sample components under ion bombardment. This effect should be taken into account during the quantitative analysis of samples and the isotope analysis by ion-beam methods. The preferential sputtering study of isotopes of an element allows to obtain a physical information about the features of atoms movement with different masses in near-surface layers of solids under ion beam bombardment. In cited papers concerning this phenomenon study the energy of bombarding ions, as a rule, is in the range from some hundreds eV to 10-15 keV.

Thus, generally the mass-spectrometer study of ion sputtering processes in a wide energy range of primary ions (up to 150-200 keV) is of physical and applied interest. Since the overwhelming majority of particles are sputtered in a neutral state (more than 99%) [8], and the neutral particle flow in equilibrium state represents the real stochiometric composition of a sputtered sample [2, 4], during the investigation of ion sputtering processes it is necessary to detect namely the flow neutral component of sputtered particles.

Presently in native and world sources there is a shortage of experimental works about mass-spectrometer study of ion sputtering processes in the energy range from 20 to 150-200 keV. This is conditioned by a shortage of corresponding experimental facility for investigation. In required devices for mass-spectrometric analysis of the flows of secondary neutral particles (both commercial and laboratory samples) on the grounds of design compactness the energy of primary beam in the ion sources is usually confined by a value of 20-30 keV. In connection with this, lots of works about the mass-spectrometric study of ion sputtering products concern just to this range of the primary ions energies. In this work we present the experimental results about the physical aspects study of ion sputtering processes in a wide range of the primary ion energies (up to 170 keV), which were carried out using our special experimental facility for mass-spectrometry of secondary neutrals.

2. EXPERIMENTAL EQUIPMENT

The experimental device is produced on the base of a high-dose ion implanter, generating ion beams with the energies up to 170 keV and current density on the sample surface up to 1 mA/cm^2. The general scheme of abovementioned device is presented in Fig. 1.

Using the ion implanter allows to obtain the mass separated beams of gaseous ions with a mass number no more than 40 with filtered neutral component of a primary beam, that is necessary for obtaining the correct data during the ion sputtering experiments. The duoplasmatron is an ion source. The ion energy in a source outlet is 20 keV, that together with potential of implanter high-voltage part (from 0 to 150 keV) defines the final energy of ion beam (inlet chamber is earthed). The residual vacuum in disposition area of the sputtered sample reaches $7 \cdot 10^{-6}$ Pa. For the vacuum conditions improvement in inlet chamber by working ion source the partition was placed (pos. 15 in Fig 1), which divided the device vacuum chamber into two sections, each of which is evacuated on high vacuum separately under open high-vacuum valve 11. The partition has a number of holes with diameter of 5 mm for ion beam passage.

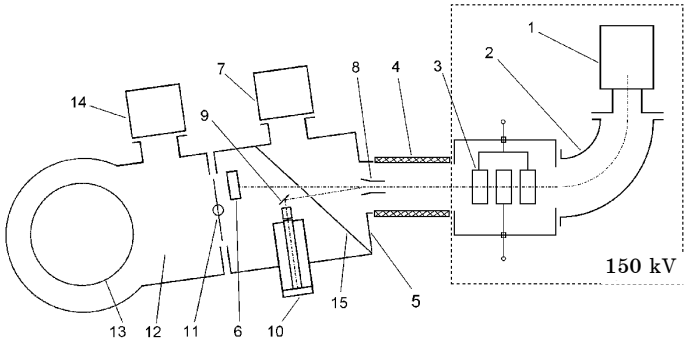

Fig. 1 *– General scheme for analysis of the secondary neutral particles (top view: 1 – ion source, 2 – electromagnet, 3 – einzel lens, 4 – accelerating tube, 5 – inlet chamber No1, 6 – Faraday cup, 7, 14 – high-vacuum pumps, 8 – plates of the beam additional turn, 9 – test sample, 10 – analysis system of sputtered particles, 11 – high-vacuum valve, 12 – inlet chamber No2, 13 – circular table for samples fastening during implantation, 15 – partition for differential pumping; primary and secondary ion trajectories are marked by the dashed-dot line)*

The analysis system of sputtered particles is built-in into a side flange of implanter inlet chamber. Structurally it can be fasten on a flange at different angles, which correspond to the angles between the primary beam axes and the system ion-optical axis, equal to 45°, 70°, or 90°. The position alignment of primary ion beam in horizontal plane is carried out using the plates of the beam additional turn. The detailed scheme of the analysis system of sputtered particles is represented in Fig. 2.

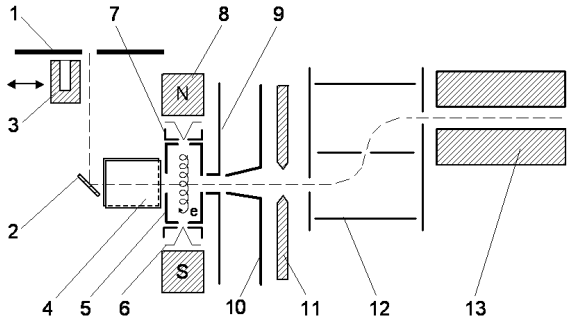

Fig. 2 *– Analysis system scheme of the sputtered particles (1 – aperture on the ion primary beam way, 2 – test sample, 3 – movable Faraday cup, 4 – secondary ion deflector, 5 – anode, 6 – cathode, 7 – reflecting electrode, 8 – permanent magnet, 9 – current controller of gaseous ions, 10 – extracting electrode, 11 – focusing electrode, 12 – electrostatic energy filter, 13 – monopole mass-analyzer; primary and secondary ion trajectories are marked by the dashed line)*

The diameter of ion beam, incident on a sample, is defined by the hole diameter in a cutting aperture (as a rule, 1-2 mm). Current measurement of

the primary ions, incident on a test sample, is realized using the movable Faraday cup, which simultaneously functions as an ion beam slider. Sputtered neutral particles are ionized (so-called, postionization of neutrals) in an ion source of the Nier-type by an electron beam of controllable energy (in the range of 50-100 eV), focused by a longitudinal magnetic field. The current of cathode electron emission is stabilized by a power unit of cathode filament circuit at the value of 0,5 or 1 mA.

One of the main factors, which define the obtained spectrum quality of postionized secondary neutrals, is a background suppression effectiveness of the secondary ions and the ions of residual vacuum medium. Intensity of such signals can exceed by some orders of magnitude the signal of postionized secondary neutrals. For a background suppression of secondary ions in a given device design the secondary ion deflector, located between the test sample and the ionizer, is used. To filter off the component of mass-spectrometric signal, connected with ions of residual gases in device vacuum volume, possessing the thermal energies of the order of 10^{-2}-10^{-1} eV, the positive potential, which is 1-2 V bigger than the anode one, applied on an aperture, located behind the anode. The degree of current suppression of secondary and gaseous ions during the secondary neutral analysis is 10^5 and 10^6, respectively.

The anode positive potential defines energy, obtained by post-ionized secondary neutrals, formed in the Nier ion source (without considering the initial neutral energies). Since the particle ionization occurs in a small volume (the diameter is about 2,5 mm) and with a small potential drop in it, the energy spread of ionized particles, generated by the given ion source, can be reduced to the minimum (about 1 eV). Extracted from a source and focused the ion beam gets into electrostatic energy filter. The main functions of the energy filter are: decreasing of the background and noise level in detector signal due to blocking of photon, high-energy ion, and neutral ingression on detector, and resolution improvement of monopole mass-analyzer due to blocking the high-energy component of power spectrum of analyzed ions as well. After energy filter ions undergo the mass separation in a mass-analyzer, taken from the serial monopole mass-spectrometer MX7304A, analyzing ions in the range from 1 to 400 amu. The secondary-electron multiplier SEM-6, operating in analog or caunter mode, was used as an ion detector. Detector part of the mass-spectrometer is shielded from the beam plasma and X-radiation ingression, because this extremely increases the background and noise level in detector signal. Our computer program carries out the mass-spectrometer control and the spectral information recording.

3. OPTIMAL PARAMETERS OF DEVICE PERFORMANCE

An advantage of the present modification of device design is that it can operate in one of three modes: secondary neutral mass-spectrometry (SNMS), secondary ion mass-spectrometry (SIMS) and gaseous medium mass-spectrometry. This essentially expands the device experimental possibilities. Mode switching is realized by the primary ion beam and the electron beam switching on/off, and by changes the potentials of some elements of ion optics of sputtered particle analyzing system. For each mode there are own optimal generic parameters, for which device sensitivity is maximal. These

parameters include the potentials of the ionization chamber (anode), of the aperture for current control of gaseous ions, of the deflector plates of secondary ions, and of the focusing electrode.

Some parameters of operation of sputtered particles detection system can be the same for all three operation modes. One of such parameters is transmission energy of energy filter. Actually it defines a range of ion energies, moving in mass-analyzer, which, in turn, defines the resolution and transmission of monopole mass-analyzer. In Fig. 3 we present some peaks, corresponding to the ions with certain mass number, which are done at different values of transmission energy of energy filter (peaks height is normalized on maximum).

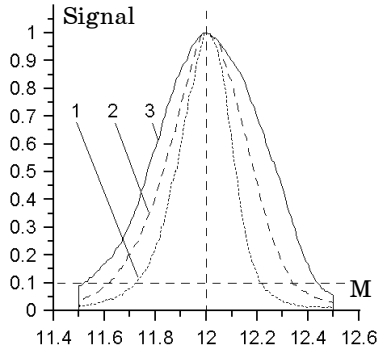

Fig. 3 *– The peaks form of monopole mass-analyzer, corresponding to the ions with certain mass number, at different values of transmission energies of energy filter (1 – 20 eV, 2 – 30 eV, 3 – 40 eV)*

According to the given figure, with the growth of the energy filter transmission energy the peak width increases, and, correspondingly, the peak resolution decreases. From another side, it was established in [9], that with the growth of the ion energy the transmission coefficient of monopole mass-spectrometer increases, and nonlinearly, and turns into saturation at the energies more than 60 eV. For study the ion sputtering processes we consider the conservation of mass-analyzer resolution (at the value of 10% from the peak height) as priority in the range from 1,5 M to 2 M, where M is the ion mass number. The ions energy, satisfying this condition, is in the range of 20-30 eV.

For an electron beam focusing in ionizer of the Nier-type we use a longitudinal (relative to the electron beam axis) magnetic field, generated by two permanent (in our case, by samarium-cobalt) magnets. The distance between magnets is 30 mm. Since using of permanent magnets there is no possibility for the rapid changes of magnetic induction in a process of mass-spectrometer measurement, for determination of magnetic field optimal value a computer simulation of electron trajectories in ionizer was used. Here for the investigated pair of magnets, located in ionizer, at first the magnetic field distribution (along the ion and electron beams axes) was experimentally measured. Measurements were made using the teslameter FH54 of Magnet-Physik Company. Then in a calculation program of charged particle trajectories the magnetic field distribution was specified so that it

corresponds to measured one. Thereafter we performed computer simulation of electron trajectories at the given values of ionizing voltage and shielding electrode potential. Software for calculation of particle trajectories was implemented in development environment Delphi. Calculation formulas are similar to those used in the well-known program SIMION. Since magnetic field is directed perpendicular to an ion flow, it deviates their trajectories, what adversely affects the ion optics transmission and, therefore, device sensitivity. So, it is necessary to minimize the magnetic field induction. On the other hand, the induction value should be sufficient for an electron beam passage without big losses through the side inlet of ionization chamber (anode). Besides, the electron beam diameter in a chamber center should not exceed the inlet diameter for neutral flow. During the experiment the optimal value of magnetic field induction in ionizer was determined, which is 34 mT in cathode peak area and 22 mT in a center of ionization chamber. We represent the corresponding magnetic field distribution diagrams in Fig. 4a and 4b and the electron trajectories in the area of their extraction at the given magnetic field distribution (in a plane passing through the ionizer center and perpendicular to the ion beam axis) in Fig. 4c.

As it is shown in Fig. 4c, at the optimal values of electrode potentials and magnetic field induction an electron beam completely passes through the side anode hole, and its diameter (due to focusing by longitudinal magnetic field) is within the inlet diameter for neutral flow and equals 1,5-2 mm.

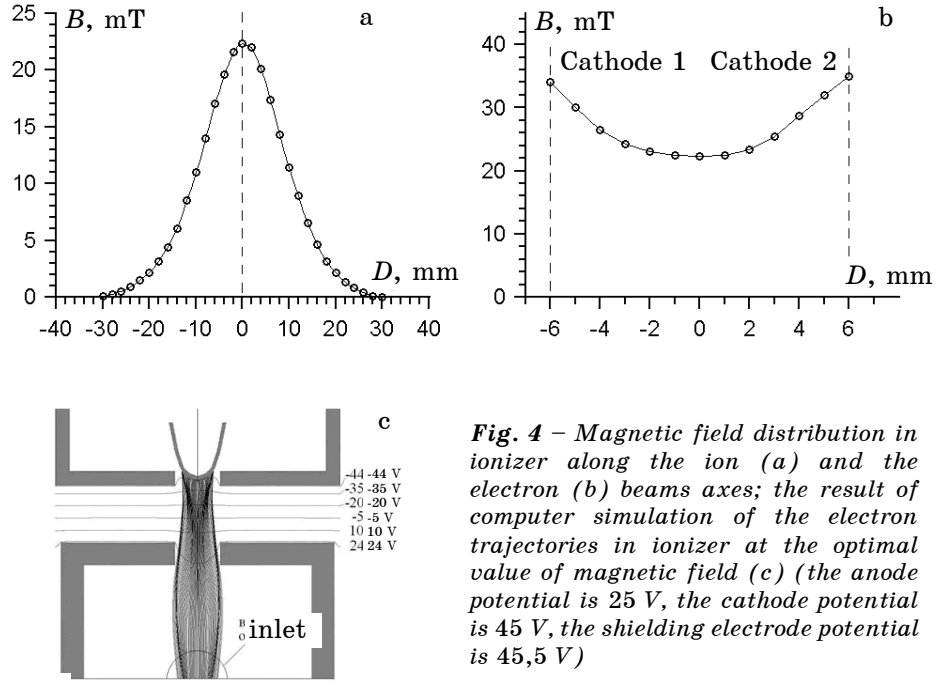

Fig. 4 *– Magnetic field distribution in ionizer along the ion (a) and the electron (b) beams axes; the result of computer simulation of the electron trajectories in ionizer at the optimal value of magnetic field (c) (the anode potential is 25 V, the cathode potential is 45 V, the shielding electrode potential is 45,5 V)*

Then the computer simulation of ion trajectories in the particle detection system was carried out and the optimal potentials of ion-optical tract

elements for each of three modes of device performance are defined. Simulation was conducted taking into account the transverse magnetic field in an ionizer area in accordance with Fig. 4.

The computer simulation results of ion trajectories, corresponding to the optimal potentials of the ion-optical system elements, are presented in Fig. 5.

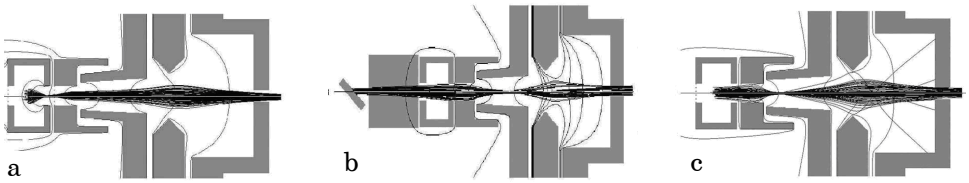

Fig. 5 *– The results of computer simulation of ion trajectories in the ion-optical system: in the mode of gas analysis (a) (the anode potential is* 30 *V, the potential of the aperture behind the anode is* 5 *V, the focusing electrode potential is* 20 *V; the ion initial energies are* 2,5·10^{-2} *eV); in the mode of secondary ions analysis (b) (the potential of the test sample is* 20 *V, the potential of deflector plates* 20 *V, the anode potential is* 15 *V, the potential of the aperture behind the anode is* 10 *V, the focusing electrode potential is* 40 *V; the ion initial energies are* 10 *eV); in the mode of secondary neutral analysis (c) (the anode potential is* 25 *V, the potential of the aperture behind the anode is* 26 *V, the focusing electrode potential is* 30 *V; the ion initial energies are* 5 *eV). In all three modes the extracting electrode potential is* 90 *V*

4. EXPERIMENTAL RESULTS

4.1 The emission study of the sputtered neutral copper clusters at different parameters of the argon primary ion beam

Under solid surface bombardment by accelerated ion beam besides the neutral and charged monoatomic particles the neutral and charged clusters are sputtered. Recently they are of a great attention in connection with rise of popularity of the sample quantitative analysis methods, based on the ion sputtering of particles from its surface, since it is necessary to take into consideration the cluster emission of a given element during the detection of the element atomic content in a sample. We have also to note the using of ion sputtering process in cluster ions sources [10-14]. In cluster sources of sputtering type it is expedient to use such parameters of primary ion beam, under which the relative clusters content in a sputtered particles flow is maximal. That is why the study of cluster emission processes at different bombardment parameters is of physical and applied interest. Almost all obtained by different authors results belong to the case of surface sputtering by ions with the energies less than 1 keV [15, 16] or some keV [17-19]. Using the proposed in this work device allows to investigate the cluster emission at higher ion energies (up to 170 keV).

In this work the results of emission study of postionized neutral copper clusters at different parameters of the Ar^+ primary ion beam (current density and energy) and emission angles of sputtered particles are represented. The study of cluster emission processes in our case is carried out by analysis of the detector ion current (corresponding to the postionized neutral copper clusters with a number of atoms n) to ion current (corresponding to the postionized copper atoms) ratio $I(Cu_n^+) / I(Cu^+)$.

Unfortunately, this ratio does not equal to the real ratio of a number of sputtered neutral particles of given types in general flow. This is connected with peculiarities of the neutral postionization process and their transport to the mass-spectrometer detector:

- the ionization effectiveness of electron impact depends not on the flow F, but on the sputtered neutral concentration ρ in ionizer; and the condition $\rho = F/\upsilon$ holds, where υ is the particle velocity (at given energy the clusters with larger mass have lesser velocities, and, correspondingly, higher concentrations in ionizer);
- the value of ionization cross-section by electron impact is specific for a given type of particle (clusters with different numbers of atoms have different ionization cross-sections);
- the mass discrimination, connected with transverse magnetic field presence;
- the mass discrimination of the monopole mass-analyzer.

Nevertheless, we can investigate the clusters emission processes, if to make an experiment at fixed settings of the sputtered particle detection system. In this case for particle flows the following relation holds:

$$\frac{F(\mathrm{Cu}_n)}{F(\mathrm{Cu})} = \frac{I(\mathrm{Cu}_n^+)}{I(\mathrm{Cu}^+)} C_n , \qquad (1)$$

where C_n is the constant for a given number n, corresponding to the certain settings of the sputtered particle detection system.

One more important question, worthy of special consideration, is the cluster dissociation influence under their postionization on the cluster relative content in a flow of analyzed particles. In this work the electron energy in ionizer was fixed at the minimal value, which is equal 50 eV. The further reduction of this value leads to significant service life decrease of cathodes. In foreign publications, devoted to the investigations of neutral cluster emission under sputtering, in [17, 19] this value of energy is used as well. Authors of these works prove that even if dissociative ionization takes place under ionization of sputtered neutral clusters of metals, it does not play an essential role. As during the electron collision a very small part of its energy is transferred to the atom cores in a cluster, only indirect processes can play the substantial role under cluster dissociation. This can be, for example, cluster stability violation due to changing of a number of electrons on the atom outer shell. It is difficult to estimate the ratio of usual and dissociative ionizations because of the lack of the corresponding experimental data for metal clusters. It is known, that for Cu_2 cluster the ionization energy-to-dissociation energy ratio I_p/D approximately equals 3. It is also known, that, for example, for H_2 molecule, having roughly the same ratio I_p/D, at the ionizing electron energy of 50 eV the dissociative ionization cross-section is 20 times less than the usual one [17]. There are other considerations about negligibility of the dissociative ionization influence as well.

During the intensity determination of the registered ion signals only those parts of mass range were scanned which contain peaks of postionized atoms and copper clusters. Then peak intensities, corresponding to the isotopes (or isotopic combinations) of a given ion type were summarized. The

primary ion current, flowing on a sample, was varying by the beam focusing using the einzel lens, located in front of the accelerating tube. Diameter of the cutting aperture in front of the test sample was 2 mm. Measurement of the primary ion current was carried out by the movable Faraday cup, located between the aperture and the sample. The mass-spectrum of postionized secondary neutrals of the copper sample is represented in Fig. 6.

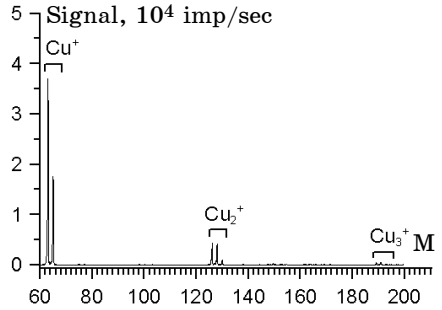

Fig. 6 *– The mass-spectrum of postionized secondary neutrals, sputtered from the copper sample (the primary ions – Ar^+, the energy is 75 keV, the current is 7 μA, electron emission current is 1 mA)*

According to obtained in the SNMS regime data the monotonic and rather abrupt decrease of the signal intensity of $I(Cu_n)$ clusters with the growth of n is observed. Here $I(Cu_{n+1}) / I(Cu_n) \sim 0{,}1$. Quite another situation is in the SIMS spectrums. Here the signal intensity periodic variation of the clusters with even and odd n takes place. And $I(Cu_{2k+1}) > I(Cu_{2k})$ for $k > 0$. Such intensity variations in the SIMS spectrums can be explained by the corresponding variations of the cluster ionization probability $\alpha(Cu_n^+)$ under sputtering in accordance with the following dependence [20]:

$$\ln[\alpha(Cu_n^+) / \alpha(Cu_n^+)] \sim E_i(Cu^+) - E_i(Cu_n^+) , \qquad (2)$$

where E_i is the effective ionization energy of the corresponding cluster. As some clusters are sputtered in excited state, the given value can be essentially smaller than the ionization energy of the "cold" cluster.

In Fig 7 we present dependencies of the signals relative intensity, corresponding to the postionized neutral copper clusters Cu_2^+ and Cu_3^+, versus the primary ion energy at the fixed primary ion current (and current density).

According to obtained figures with the growth of bombarding ion energy in the range of 30-170 keV the cluster relative intensity decreases. Here the falling velocity of the relative intensity of Cu_3^+ is higher. Such curve behavior can be explained from the point of view of the so-called atomic combination mechanism (ACM). This is a statistical model, which was very useful for study of the metal surface sputtering by inert gas ions. For the first time the given model was proposed in the work [21] and was independently developed by Konnen [22] and Gerhard [23]. According to this model the sputtered particle formation (including clusters) passes as following. Two or more not just nearest surface atoms, individually knocked-on under double collisions in one collision cascade, can join together during the yield from the surface, if their impulses are mutually agreed so that the formed

molecule is energy-wise more preferential in comparison with the single atoms. The probability of such joining and, correspondingly, the sputtering coefficient of a cluster with n atoms $Y(X_n)$ is determined by relation

$$Y(X_n) \sim (Y_{total})^n. \quad (3)$$

The total sputtering coefficient Y_{total} is defined by expression

$$Y_{total} = \sum_{n=1}^{\infty} nY(X_n) \approx Y(X) + 2Y(X_2). \quad (4)$$

In general case the sputtering coefficients, entered into the equations (3) and (4), depend on the energy and the incidence angle of primary ions.

For determination the total copper sputtering coefficient as a function of energy of bombarding argon ions the computer simulation with the SRIM program was used. Obtained dependence is represented in Fig. 8.

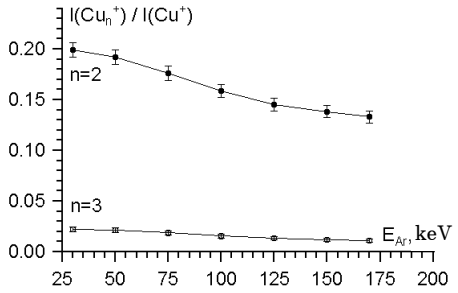

Fig 7 *– Dependencies of the signal relative intensity, corresponding to the postionized neutral copper clusters Cu_2^+ and Cu_3^+ versus the primary ion energy (the primary ions – Ar^+, the current is 7 μA, the incidence angle is 45°, the angle of particle collection is 0°, the impulse accumulation time under Cu^+ and Cu_2^+ registration is 200 msec, under Cu_3^+ registration is 2000 msec)*

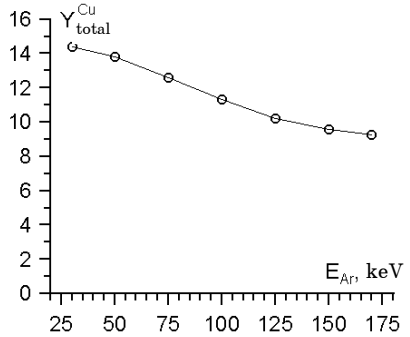

Fig. 8 *– Dependence of the total copper sputtering coefficient versus the energy of bombarding argon ions at the incidence angle of 45° (computer simulation with the SRIM program)*

Sputtering coefficient in each point of dependence is defined by the launching of 10^4 ions that corresponds to statistical estimation error of the order of 1%. According to the figure the sputtering coefficient in the energy range from 30 to 170 keV monotonically decreases with the growth of the primary ion energy.

Using formulas (3) and (4) and taking into account (1), where the particle flow F can be replaced by their partial sputtering coefficient Y, in general case for the Cu_n ($n > 2$) cluster we obtain the following relation:

$$\sqrt[n-1]{\frac{I(Cu_n^+)}{I(Cu^+)}} \sim Y_{total} \sqrt[n-1]{1 + \frac{2I(Cu_2^+)}{I(Cu^+)} C_2} . \qquad (5)$$

For the estimation of the calibration factor C_2, depending on the settings of neutral particle detection system, we used the experimental results of [19], where there is the data about relative content of sputtered neutral clusters of silver and copper at the Ar^+ ion beam energy of 5 keV and the incidence angle of 45°. As the minimal energy of the ion beam, generated by ion implanter, is in the range of 20-30 keV, for the reconstruction of the necessary ion beam parameters the sputtered particle detection system was placed on the other device, representing the ion source test stand. Installed in it the ion source could generate the argon ion beams with energies in the range of 1-15 keV. Comparing the peak intensities of the Cu_2 cluster in obtained on the stand spectrum and the data of [19] the coefficient C_2 is calculated and equals 0,94. The similar coefficient for the Cu_3 cluster is $C_3 = 0{,}91$.

As an example we consider the case, when $n = 3$ in the formula (5). The expression $[1+2C_2I(Cu_2^+)/I(Cu^+)]^{1/2}$ weekly depends on the primary ion energy. So, according to Fig. 7, during the energy change from 30 to 170 keV it varies by 4%, while the total copper sputtering coefficient Y_{total} according to Fig. 8 varies by 40%. Thus, according to recombination model the square root of the relative intensity of the Cu_3 cluster signal in first approximation is proportional to the total copper sputtering coefficient. The corresponding diagram, plotted on the base of the points in Fig. 7 and 8, is represented in Fig. 9.

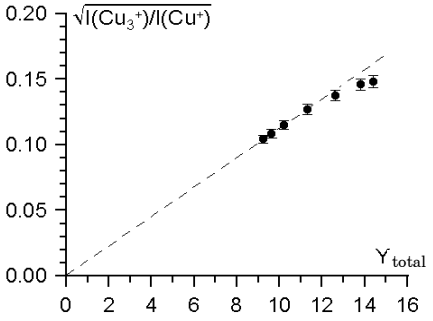

Fig. 9 *– Dependence diagram of the $[I(Cu_3^+)/I(Cu^+)]^{1/2}$ versus the total copper sputtering coefficient Y_{total}*

According to this diagram the linear dependence really takes place up to $Y_{total} \cong 11$. But at higher values of Y_{total} the significant deviation from linearity and gradual transition to the saturation region are observed. This means that recombination model of clusters formation becomes unusable at high values of the metal sputtering coefficients.

Dependencies of relative intensity of the signals, corresponding to the postionized neutral Cu_2^+ and Cu_3^+ clusters, on the particle emission angle (see Fig. 10) were obtained as well. The emission angle setting was performed before the experiment by fastening the secondary particle detection system at the necessary angle on a side flange of the inlet chamber. In this case the effective semiangle of secondary neutral collection was approximately 5°. Measurements were carried out at fixed values of the energy, the current density, and the incidence angle of a primary ion beam, and the settings of the particles detection system as well. According to the obtained data with the particle emission angle growth the cluster relative content in a sputtered particle flow strongly decreases and the relative reduction rate of the content is higher for clusters with larger n.

This can be explained by the differences in angular distributions of clusters with different n. Recombination model of clusters formation under sputtering shows, that if angular distribution of sputtered atoms can be described by the function $f(\theta)$ then the similar distribution for the cluster with a number of atoms n will be described by the function $f^n(\theta)$, that is it will be more extended along the surface normal, what is confirmed by the dependences in Fig. 10.

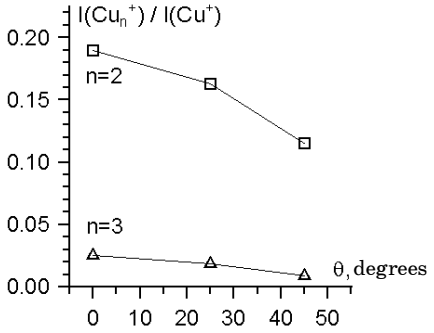

Fig. 10 *– Dependence of relative intensity of the signals, corresponding to the postionized neutral Cu_2^+ and Cu_3^+ copper clusters versus the particle emission angle (the primary ions – Ar^+, the energy is 75 keV, the incidence angle is 45°, the current density is 0,3 mA/cm², the impulse accumulation time under Cu^+ and Cu_2^+ registration is 200 msec, under Cu_3^+ registration is 2000 msec)*

Dependences of relative intensities of the signals, corresponding to the postionized neutral Cu_2^+ and Cu_3^+ copper clusters, on the current density of argon primary ions at the fixed primary ion energy are represented in Fig. 11. As the ion beam width essentially exceeds the diameter of cutting aperture, the profile of that part of the beam, which is cutout by the aperture, can be considered as smooth, and the current density value can be found by the formula

$$j_{Ar} = \frac{I_{Ar}\cos\alpha}{S} = \frac{4I_{Ar}\cos\alpha}{\pi d^2}, \qquad (6)$$

where I_{Ar} is the primary ion current, passing through the cutting aperture and measurable by the movable Faraday cup, S is the aperture hole area, d is the aperture diameter (2 mm), α is the incidence angle of the primary ion beam (45°).

According to Fig. 11 the cluster relative current intensity with the growth of the current density of primary ion beam monotonically increases, and the relative intensity of the Cu_3^+ increases stronger (almost two times during the current growth from 0,05 to 0,45 mA/cm^2). This is explained by the fact that with the growth of the beam current density the density of the sputtered copper atoms increases near the sample surface, and this means the increasing of their recombination probability. Here the more the number of atoms in cluster, the stronger the probability increase of the given cluster formation with the current density growth.

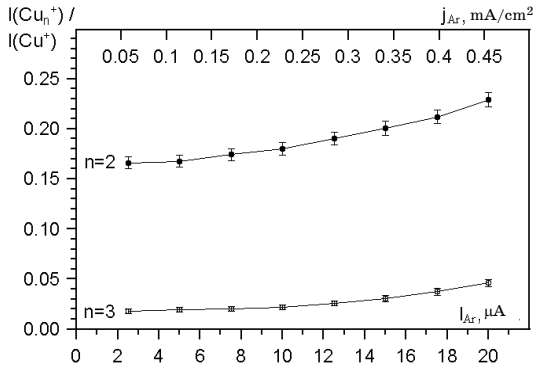

Fig. 11 *– Dependencies of relative intensity of the signals, corresponding to the postionized neutral Cu_2^+ and Cu_3^+ copper clusters versus the primary ion current (current density) (the primary ions – Ar^+, the energy is 75 keV, the incidence angle is 45°, the angle of particles collection is 0°, the impulse accumulation time under Cu^+ and Cu_2^+ registration is 200 msec, under Cu_3^+ registration is 2000 msec)*

4.2 The study of preferential sputtering effect of the molybdenum isotopes under ion bombardment

The sputtering process of solids by accelerated ion flow has a number of characteristic properties, and the one of which is the so-called preferential sputtering effect. It consists in that for a multicomponent material the particle flow composition emitted in the sputtering process can differ from the target stoichiometric composition [2]. Furthermore, it is found that this effect appears even on the level of different isotopes of the same element [24]. For the multicomponent materials besides the differences in component masses, the effect of the component chemical bond [25] is an important and dominant in this phenomenon. And for isotopes of an element this phenomenon connected solely with their difference in mass. Proposed by Sigmund the analytical theory of preferential sputtering [26, 27], based on a

concept of linear collision cascades [28], predicts that for two isotopes of an element with the mass numbers M_1 and M_2 and the bulk concentrations C_1 и C_2 in homogeneous sample the ratio of their sputtering coefficients under small fluences of bombarding ions $(Y_1/Y_2)_0$ is defined by the relation

$$\left(\frac{Y_1}{Y_2}\right)_0 = \frac{C_1}{C_2}\left(\frac{M_2}{M_1}\right)^{2m}, \tag{7}$$

where parameter m characterizes the interatomic interaction potential in power approximation ($0 < m < 1$). As in the equilibrium state under sputtering $(Y_1/Y_2)_\infty = C_1/C_2$ the equation (7) defines the initial deviation of the sputtered particle flow composition form the bulk stoichiometry, the value of isotopic enrichment is characterized by the following parameter:

$$\delta_0 = \frac{(Y_1/Y_2)_0}{(Y_1/Y_2)_\infty} - 1 = \left(\frac{M_2}{M_1}\right)^{2m} - 1. \tag{8}$$

Enrichment of sputtered particle flow by a lighter isotope is observed in the beginning of the ion sputtering process. During the sputtering process this enrichment decreases, and finally the equilibrium is reached. In this case the ratio of these isotopes on a sample surface differs from the bulk ratio by the value of δ_0^{-1}.

There are a lot of publications in the world sources, devoted to the experimental study of the isotope preferential sputtering, carried out using both the SNMS method [29-31] and the SIMS method [32-36]. In most of these works the ions with energies not exceeding 20 keV are used. Represented in this work device allows to perform investigation of the preferential sputtering effect under ion bombardment with higher energies (up to 170 keV). The using of SNMS regime is more preferred in our case than the SIMS regime. This is connected with that in SIMS regime the peak intensity of two studied isotopes is defined by their ionization coefficients under sputtering β_1 and β_2, which in general case are not equal and are the velocity functions of corresponding atoms in the moment of their sputtering from a sample surface [32, 37]. It is well known, that the intensity of secondary ion emission strongly depends on the sample surface condition. During the ion sputtering the variation of the coefficients β_1 and β_2 can essentially deform the measurable peak ratio of two isotopes. Operating in SNMS regime, the ion current ratio of two isotopes (under constant primary ion current condition) is given by the relation

$$\frac{I_1}{I_2} = \frac{Y_1}{Y_2}\frac{P_1}{P_2}\frac{T_1}{T_2}, \tag{9}$$

where P_i and T_i are, respectively, the ionization probability and the total transmission coefficient of ion-optical system for the isotope i. Due to energy filter using the ions within the certain energy range get into mass-analyzer. For two isotopes of an element with different mass numbers M_1 and M_2 their velocities are $v_1 \neq v_2$, and therefore $P_1 \neq P_2$. As the monopole

mass-analyzer transmission depends on a mass number of considered ion and, besides, there is a transverse magnetic field in ionizer, then $T_1 \neq T_2$. So, the ratio of isotope peak intensities will differ from the real relation of isotopes in sputtered particle flow by a certain factor, which is defined by the ion-optical system parameters. If the ion-optical system parameters are fixed during the sample sputtering then (P_1/P_2) (T_1/T_2) = const. Taking this into account and substituting (9) in (8), we obtain the formula for the isotopic enrichment parameter, expressed in terms of ion currents of two isotopes I_1 and I_2, which are registered by mass-spectrometer detector

$$\delta_0 = \frac{(I_1/I_2)_0}{(I_1/I_2)_\infty} - 1. \qquad (10)$$

As we want to obtain the maximal values of enrichment parameter ψ_0, then according to the equation (8) it is necessary to select such element of periodic system, which has two stable isotopes with the maximal ratio of their mass numbers M_2/M_1. Besides the isotopes with mass numbers $M_1 - 1$ and $M_2 - 1$ should be absent, that is the peaks of their hydrides can be superimposed on the peaks of studied isotopes. The listed above conditions satisfies germanium (^{70}Ge and ^{76}Ge) and molybdenum (^{92}Mo and ^{100}Mo). In our case the molybdenum was studied, the isotope spectrum of which is represented in Fig. 12.

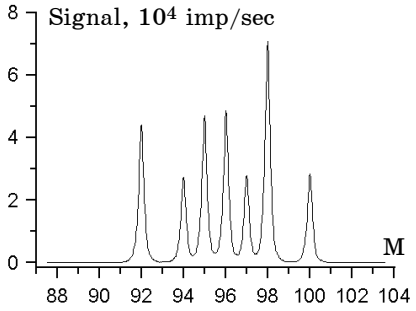

Fig. 12 *– Mass-spectrum of the molybdenum isotopes, obtained in SNMS regime in the equilibrium state under sputtering (the primary ions – Ar^+, the energy is* 80 *keV, the current is* 10 *μA, the incidence angle is* 45°*, the angle of sputtering particles collection is* 0°*, the electron emission current is* 1 *mA, the impulse accumulation time is* 500 *msec)*

According to this spectrum in the equilibrium state the ^{92}Mo-to-^{100}Mo isotope peak height ratio is 1,529 ± 0,002. In accordance with the table data about the content of isotopes in nature [38] the ^{92}Mo-to-^{100}Mo isotope peak height ratio is 1,540. Discrepancy in these values is conditioned by different sensitivity for two given isotopes in SNMS regime, and by error estimation of peak intensity as well. As in SNMS method the particles, sputtering within the certain spatial angle, are registered, the difference of angle distributions for particles with different masses influences on the given isotope ratio.

Before placing the molybdenum samples into working chamber they were released from the oxide layer by dipping in hydrochloric acid. Then they were rinsed by water, ethanol and dried in drying box. During experiments the samples temperature was 150-200°C for surface degassing. Before measurements the mass scale calibration was specified for that the studied peaks exactly correspond to their mass numbers. To decrease the measurement error of peak intensity it is necessary to use large times of impulse accumulation (more than 1 sec). Otherwise, the time of spectrum obtaining of two studied peaks should be small enough (some seconds) in order that the primary ion current drift has no effect on a measured peak ratio. To provide a high velocity of peak scanning at large time of impulse accumulation, the regime of selective scanning was used, that is the signal intensity was measured in the peak neighborhood only. In this case the time of one spectrum obtaining with two peaks was about 12 sec at the time of impulse accumulation of 3 sec. In order that the signal intensities of two isotopes during their ratio determination correspond to the same time moment of these signals registration the linear interpolation of two adjacent isotope signal values in array of a type the signal value/the time of its measurement (separately for every isotope) was used.

The aperture diameter, specified the beam size on a sample surface, was 1,5 mm. The ion beam current during the experiment was constant and equal 2,5 $\mu A/cm^2$, that corresponded the current density on a sample surface of 0,1 mA/cm^2. As an ion beam during measurements was strongly defocused by the einzel lens, the beam diameter (about 30 mm) essentially exceeded the diameter of cutting aperture. This means that the beam profile, passing through the aperture, is closed to rectangular form, that allows to minimize the so-called "crater effect", which leads to an inaccuracy in obtained results under sample sputtering.

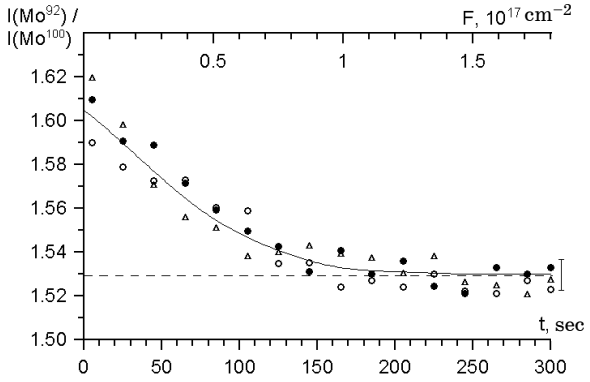

***Fig. 13** – Diagram of the I(^{92}Mo) / I(^{100}Mo) molybdenum isotope signals ratio versus the ion fluence F and sputtering time t (the primary ions – Ar^+, the energy is 80 keV, the incidence angle is 45°, the angle of sputtering particles collection is 0°)*

In Fig. 13 we present the experimentally obtained dependence of the ^{92}Mo-to-^{100}Mo molybdenum isotope signal ratio versus the primary ion fluence. We have done 3 sets of measurements on different molybdenum samples. The ion fluence was calculated using the measurement time of the

isotope signal ratio and the ion current density, flowing on a sample. The value of isotopic enrichment parameter ψ_0, calculated on the base of the formula (10), in this case is $(4{,}9 \pm 0{,}6)\cdot 10^{-2}$. The equilibrium state is approximately reached in 230 sec that corresponds to the ion fluence $F_{st} = 1{,}37\cdot 10^{17}$ cm^{-2}. The depth d_{st} of equilibrium state reaching can be found with the formula

$$d_{st} = \frac{j_{Ar}\, Y_{Mo}\, m_{Mo}\, t}{e\, \rho_{Mo}}, \qquad (11)$$

where j_{Ar} is the current density of argon primary ions Ar^+ ($j_{Ar} = 10^{-4}$ A/cm^2), Y_{Mo} is the molybdenum sputtering coefficient at the given energy and the incidence angle of argon ion beam ($Y_{Mo} = 5{,}7$ based on computer simulation using the SRIM program), m_{Mo} is the molybdenum atomic mass ($m_{Mo} = 1{,}6\cdot 10^{-22}$ g), t is the sputtering time, corresponding to the equilibrium state ($t \approx 220$ sec), e is the electron charge ($e = 1{,}6\cdot 10^{-19}$ C), ρ_{Mo} is the molybdenum density ($\rho_{Mo} = 10{,}2$ g/cm^2). Substituting these values we obtain $d_{st} = 1{,}23\cdot 10^{-5}$ cm = 1230 Å.

Dependences of the I(^{92}Mo) / I(^{100}Mo) isotope signal ratio versus the ion fluence are obtained at other values of bombarding ions energy as well. The results based on these dependences are presented in Table 1.

Table 1 *– Investigation results of the preferential sputtering in a pair ^{92}Mo-^{100}Mo at different energies of primary ions E_{Ar} (the beam incidence angle is 45°, the angle of particle accumulation is 0°)*

E_{Ar}	30	80	130	170
δ_0, %	5,2 ± 0,6	4,9 ± 0,6	4,7 ± 0,6	5,1 ± 0,6
m	0,30	0,29	0,28	0,30
F_{st}, cm^{-2}	$6{,}3\cdot 10^{16}$	$1{,}4\cdot 10^{17}$	$2{,}2\cdot 10^{17}$	$2{,}7\cdot 10^{17}$
Y_{Mo} (45°)	6,4	5,7	5,1	4,8
d_{st}, Å	640	1230	1728	2030
R_p, Å	200	430	640	810

According to these results with growth of the bombarding ion energy the value of parameter δ_0 remains approximately constant. Obtained depth values d_{st}, on which it is necessary to sputter the sample for transition to the stationary sputtering regime, essentially exceed the average depth of sputtered atom emission (of the order of 1 nm [1, 4]). Besides, this value increases with growth of the primary ion energy. This means that apart from the preferential sputtering process the two attendant transfer mechanisms, namely, the recoil atom implantation under collisions and the cascade atom mixing under action of ion bombarding, essentially influence on the isotopic composition of sputtered atom flow. This leads to migration towards the surface of atoms of deep-seated layers, which have a natural isotope composition. The action of these processes is spread out to the depth comparable with the primary ion range in a sample material, which value

increases with growth of the primary ion energy. To find the value of ion range in the studied samples we used computer simulation with the SRIM program. The ion range R_p was defined as a sum of normal components of the average penetration depth and straggling. According to the table data the depth, on which the equilibrium is reached, at the average 2,5-3 times exceeds the ion range. These results can be compared, for example, with the ones obtained in the work [30], where investigations are carried out by the SNMS method of molybdenum preferential sputtering by argon atoms at low primary ion energies (5 keV). In accordance with these results the stationary state is reached at the ion fluence of $6 \cdot 10^{16}$ cm^{-2}. Here the depth, on which the stationary state is reached, exceeds 4 times the ion range.

The study of dependence of isotopic enrichment factor on the sputtered particle emission angle under other equal conditions was carried out as well (see Fig.14). According to obtained data the isotopic ratio and the value of isotopic enrichment factor decrease with the growth of the sputtered particle emission angle.

Computer simulation with the specially developed programs (OKSANA, TRIDYN, TRIM.SP and others) is widely used for studying the processes of preferential sputtering. In our case for the obtained experimental data verification we used the results of computer simulation of preferential sputtering the molybdenum isotopes under Ar^+ bombarding with ion energies in the range from 0,1 to 100 keV, done by Shulga in [39]. In this work simulation was carried out with OKSANA program, described in detail in [40-42]. One result of this simulation is represented in Fig. 15.

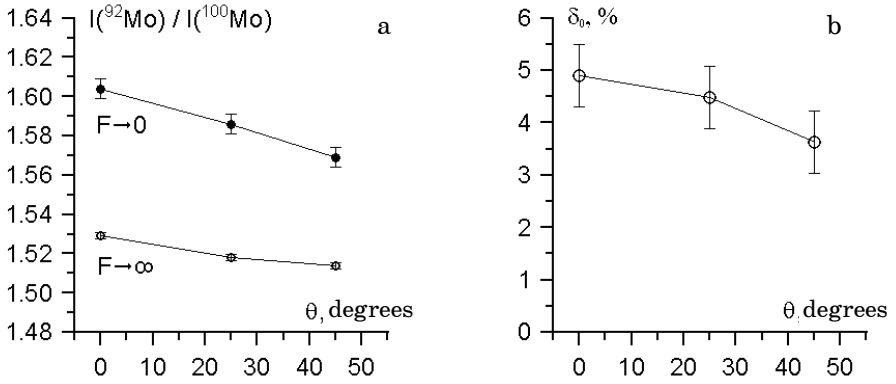

Fig. 14 *– Dependences of the intensity ratio of the $I(^{92}Mo)$ / $I(^{100}Mo)$ molybde-num isotope signals within zero and infinite primary ion fluence F, and the corresponding isotopic enrichment factor δ_0 versus the sputtered particle emission angle θ (the primary ions – Ar^+, the energy is 80 keV, the incidence angle is 45°)*

According to the present diagram the largest values of the coefficient m and correspondingly of the isotopic enrichment factor δ_0 are observed at the ion energies near the threshold ones for ion sputtering (of the order of 100 eV). With the ion energy growth in the range from 0,1 to some keV these values essentially decrease and, starting from the energy about 10 keV, transit to the stationary state. This corresponds to the data obtained experimentally (Table 1), according to which in the range of ion energies

from 30 to 170 keV the isotopic enrichment factor remains stable. The results of computer simulation also show, that with growth of the particle emission angle the coefficients m and δ_0 decrease, that is in accordance with our experimental data (see Fig. 14).

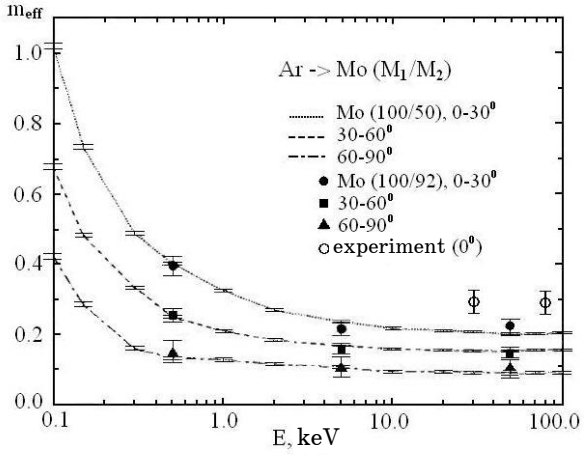

Fig. 15 *– Dependence of the effective coefficient m versus the energy of bombarding ions Ar^+ for three intervals of sputtered particle emission angles (computer simulation, isotopic mixtures $^{100}Mo/^{50}Mo$ and $^{100}Mo/^{92}Mo$ in proportion 1:1, for comparing our experimental results are given in this diagram as well)*

The effective value of the coefficient m, obtained during our experiment, is about 0,29 for the ion energies of some tens keV and emission angle $\theta = 0°$ (more exactly $\theta = 0\text{-}5°$ taking into account the value of sputtered particle capture angle by analysis system). It slightly exceeds the corresponding value, obtained during the simulation ($m \approx 0{,}23$ for emission angles 0-30°). But we have to note, that simulation was carried out for a wide range of emission angles, and since with emission angle growth the isotopic enrichment of sputtered particles flow decreases then the average value of coefficient m will be less than for the angle $\theta = 0°$. Effective values of the parameter m, obtained in this and other experimental works [30, 35, 36], and during the simulations [39-45] as well, are essentially higher than the theoretical value, proposed by Sigmund ($m = 0{,}055$) and corresponding to the Born-Mayer interaction potential [26]. Besides, Sigmund theory does not provide dependencies of the isotopic enrichment factor on the sputtered particles emission angle. According to the given theory the main reason of isotopic enrichment generation during sputtering is the difference in scattering cross-sections of atoms with different masses in collision cascades. Significant discrepancies of experimental and theoretical values are explained in above-listed works by a number of shortcomings and simplifications of Sigmund theoretical model, in particular, by neglect of surface effects. The dominant factor in the preferential sputtering process according to computer simulation is asymmetry of distribution of impulses between the light and heavy atoms in collision cascades. The part of light atoms, transferring impulse along the sample surface, is essentially higher than of the heavy ones. This is connected with that the more light atoms in collision cascade can scatter within the larger range of angles during collisions with the more heavy atoms. An important role in formation of sputtered particles angular distributions, according to simulation, plays their interaction with the surface barrier attractive field as well.

5. CONCLUSIONS

1. For study the ion sputtering processes at high primary ions energies the experimental device for mass-spectrometric analysis of the flows of secondary neutral particles is built. In contrast to the traditional devices of such type the primary ion source in it is a high-dose ion implanter, generating the mass separated ion beams with energies in the range from 20 to 170 keV and current density on the studied sample up to 1 mA/cm^2.
2. Operation ability in one of three modes (SNMS, SIMS and gaseous medium analysis) essentially increases the experimental possibilities of device. For each operating mode the computer simulation of ion trajectories in the analysis system of sputtered particles is done and the optimal potentials of ion optics elements are defined. The optimal ion energies in mass-analyzer (20-30 eV) and the optimal value of magnetic field in ionizer (22 mT in the ionizer center) are determined as well.
3. Investigations of emission of the neutral copper clusters Cu_n (n = 2, 3) under sample sputtering by high-energy Ar^+ ion beam are carried out. According to obtained results with the growth of primary ion energy in the range from 30 to 170 keV the relative content of neutral clusters in particle flow decreases, and the relative velocity of decreasing is higher for cluster Cu_3. Decrease of the cluster relative fraction is observed under increasing of sputtered particle emission angle as well. With the growth of current density of primary ion beam the cluster fraction increases, that is connected with the growth of sputtered atom density near the sample surface. Obtained results are in accordance with theoretical concepts of cluster formation under sputtering.
4. Investigations of isotope preferential sputtering on the example of the pair ^{92}Mo-^{100}Mo under sputtering of molybdenum sample by the high-energy Ar^+ ion beam are carried out. At small fluences of primary ions (less than 10^{17} cm^{-2}) the increased content of the lighter isotope in sputtered particle flow is observed. With the growth of primary ion energy in the range from 30 to 170 keV increases the depth, on which it is necessary to sputter the sample for sputtering process transformation to the stationary mode, and the ion beam fluence, corresponding to this depth, increases as well, and the isotope enrichment factor remains constant (at an average, about 5%). Decreasing of the isotope enrichment factor with the growth of the sputtered particle emission angle was also revealed. Obtained experimental data are in a good agreement with results of computer simulation of the preferential sputtering processes.

REFERENCES

1. R. Berish, *Raspylenie tverdyh tel ionnoy bombardirovkoy. Fizicheskoe raspylenie odnoelementnyh tverdyh tel* (M.: Mir: 1984).
2. R. Berish, *Raspylenie tverdyh tel ionnoy bombardirovkoy. Vypusk 2: Raspylenie splavov i soedineniy, raspylenie pod deystviem elektronov i neytronov, rel'ef poverhnosti* (M.: Mir: 1986).
3. R. Berish, K. Vittmak, *Raspylenie pod deystviem bombardirovki chastitsami. Vypusk 3: Kharakteristiki raspylennyh chasyits, primeneniya v tehnike* (M.: Mir: 1998).
4. V.V. Pletnev, *Itogi nauki i tehniki. Seriya: Puchki zaryazhennyh chastits i tverdoe telo* (M.: VINITI: 1991).

5. E.S. Mashkova, *Fundamental'nye i prikladnye aspekty raspyleniya tverdyh tel* (M.: Mir: 1989).
6. H. Oechsner, *Appl. Phys. A* **8** No3, 185 (1975).
7. V.S. Smentkowski, *Prog. Surf. Sci.* **64**, 1 (2000).
8. V.T. Cherepin, *Ionny mikrozondovy analiz* (K.: Naukova dumka: 1992).
9. V.A. Baturin, S.A. Yeryomin, *Visnyk SumDU. Seriya Fizyka, matematyka, mekhanika* No2, 127 (2007).
10. P. Fayet, F. Patthey, H.-V. Roy, Th. Detzel, *Surf. Sci.* **269-270**, 1101 (1992).
11. H.O. Lutz, K.H. Meiwes-Broer, *Nucl. Instrum. Meth. B* **53** No4, 395 (1991).
12. P. Fayet, L. Woste, *Zeit. Phys. D* **3** No2-3, 177 (1986).
13. H. Haberland, M. Karrais, M. Mall, *Zeit. Phys. D* **20** No1-4, 413 (1991).
14. W. Begemann, R. Hector, Y.Y. Liu, J. Tiggesbaumker, *Zeit. Phys. D* **12** No1-4, 229 (1989).
15. H. Gnaser, H. Oechsner, *Nucl. Instrum. Meth. B* **82** No2, 347 (1993).
16. H. Gnaser, H. Oechsner, *Nucl. Instrum. Meth. B* **58** No3-4, 438 (1991).
17. J. Schou, W.O. Hofer, *Appl. Surf. Sci.* **10** No3, 383 (1982).
18. K. Franzreb, A. Wucher, H. Oechsner, *Nucl. Instrum. Meth. B* **17** No1, 51 (1990).
19. K. Franzreb, A. Wucher, H. Oechsner, *Surf. Sci. Lett.* **279** No3, L225 (1992).
20. K. Franzreb, A. Wucher, H. Oechsner, *Phys. Rev. B* **43** No18, 14396 (1991).
21. H. Oechsner, H. Gerhard, *Sur. Sci.* **44** No2, 480 (1974).
22. G.P. Konnen, A. Tip, A.E. de Vries, *Radiation Effects* **21** No4, 269 (1974).
23. W. Gerhard, *Zeit. Phys. B* **22** No1, 31 (1975).
24. G.K. Wehner, *Appl. Phys. Lett.* **30** No4, 185 (1977).
25. H.H. Andersen, B. Stenum, T. Sorensen, H.J. Whitlow, *Nucl. Instrum. Meth. B* **2** No1-3, 601 (1984).
26. P. Sigmund, *Nucl. Instrum. Meth. B* **18** No1-6, 375 (1986).
27. P. Sigmund, *Nucl. Instrum. Meth. B* **82** No2, 242 (1993).
28. P. Sigmund, *Phys. Rev.* **184** No2, 383 (1969).
29. H. Gnaser, *Nucl. Instrum. Meth. B* **48** No1-4, 544 (1990).
30. H. Gnaser, H. Oechsner, *Phys. Rev. Lett.* 63 No24, 2673 (1989).
31. W. Bieck, H. Gnaser, H. Oechsner, *Nucl. Instrum. Meth. B* **101** No4, 335 (1995).
32. H. Gnaser, I.D. Hutcheon, *Surf. Sci.* **195** No3, 499 (1988).
33. N. Shimizu, S.R. Hart, *J. Appl. Phys.* **53** No3, 1303 (1982).
34. V. Shutthanandan, J. Zhang, P. Ray, *J. Appl. Phys. A* **76** No7, 1093 (2003).
35. L.M. Baumel, M.R. Weller, T.A. Tombrello, *Nucl. Instrum. Meth. B* **34** No4, 427 (1988).
36. D.L. Weathers, S.J. Spicklemire, T.A. Tombrello, I.D. Hutcheon, *Nucl. Instrum. Meth. B* **73** No2, 135 (1993).
37. H. Gnaser, I.D. Hutcheon, *Phys. Rev. B* **35** No2, 877 (1987).
38. K. Rosman, P. Taylor, *Pure Appl. Chem.* **70** No1, 217 (1998).
39. V.I. Shulga, *Radiat. Eff. Defect. S.* **142** No1, 351 (1997).
40. V.I. Shulga, *Radiat. Eff. Defect. S.* **70** No1, 65 (1983).
41. V.I. Shulga, *Radiat. Eff. Defect. S.* **82** No3, 169 (1984).
42. V.I. Shulga, *Radiat. Eff. Defect. S.* **84** No1, 1 (1985).
43. W. Eckstein, J.P. Biersack, *Appl. Phys. A* **37** No2, 95 (1985).
44. M.H. Shapiro, P.K. Haff, T.A. Tombrello, E.Jr. Harrison, *Nucl. Instrum. Meth. B* **12** No1, 137 (1985).
45. M.H. Shapiro, T.A. Tombrello, E.Jr. Harrison, *Nucl. Instrum. Meth. B* **30** No2, 152 (1988).